Lithocholic acid, a bacterial metabolite reduces breast cancer cell proliferation and aggressiveness

Edit Mikó, András Vida, Tünde Kovács, Gyula Ujlaki, György Trencsényi, Judit Márton, Zsanett Sári, Patrik Kovács, Anita Boratkó, Zoltán Hujber, Tamás Csonka, Péter Antal-Szalmás, Mitsuhiro Watanabe, Imre Gombos, Balazs Csoka, Borbála Kiss, László Vígh, Judit Szabó, Gábor Méhes, Anna Sebestyén, James J. Goedert, Péter Bai

PII: S0005-2728(18)30074-4
DOI: doi:10.1016/j.bbabio.2018.04.002
Reference: BBABIO 47901

To appear in:

Received date: 19 December 2017
Revised date: 22 March 2018
Accepted date: 9 April 2018

Please cite this article as: Edit Mikó, András Vida, Tünde Kovács, Gyula Ujlaki, György Trencsényi, Judit Márton, Zsanett Sári, Patrik Kovács, Anita Boratkó, Zoltán Hujber, Tamás Csonka, Péter Antal-Szalmás, Mitsuhiro Watanabe, Imre Gombos, Balazs Csoka, Borbála Kiss, László Vígh, Judit Szabó, Gábor Méhes, Anna Sebestyén, James J. Goedert, Péter Bai , Lithocholic acid, a bacterial metabolite reduces breast cancer cell proliferation and aggressiveness. The address for the corresponding author was captured as affiliation for all authors. Please check if appropriate. Bbabio(2018), doi:10.1016/j.bbabio.2018.04.002

Lithocholic acid, a bacterial metabolite reduces breast cancer cell proliferation and aggressiveness

Edit Mikó[1,8], András Vida[1,8], Tünde Kovács[1], Gyula Ujlaki[1], György Trencsényi[2], Judit Márton[1], Zsanett Sári[1], Patrik Kovács[1], Anita Boratkó[1], Zoltán Hujber[9], Tamás Csonka[3], Péter Antal-Szalmás[4], Mitsuhiro Watanabe[10], Imre Gombos[11], Balazs Csoka[12], Borbála Kiss[7], László Vígh[11], Judit Szabó[5], Gábor Méhes[3], Anna Sebestyén[9], James J. Goedert[13], Péter Bai[1,6,8,*]

Departments of [1]Medical Chemistry, [2]Medical Imaging, [3]Pathology, [4]Laboratory Medicine, [5]Microbiology, [6]Research Center for Molecular Medicine and [7]Dermatology, Faculty of Medicine, University of Debrecen, 4032, Hungary;

[8]MTA-DE Lendület Laboratory of Cellular Metabolism, Debrecen, 4032, Hungary;

[9]1st Department of Pathology and Experimental Cancer Research, Semmelweis University, Budapest, 1085, Hungary;

[10]Department of Internal Medicine, School of Medicine, Keio University Endo, Fujisawa-shi, Kanagawa, 252-0882, Japan;

[11]Biological Research Center, 6701, Szeged, Hungary;

[12]Deptartment of Anesthesiology, Columbia University Medical Center, New York, NY 10032, USA

[13]National Cancer Institute, National Institutes of Health, Bethesda, 20982 MD, USA

Running title: Lithocholic acid modulates breast cancer

*Whom correspondence should be sent to:
Peter Bai, PhD, DSc University of Debrecen, Department of Medical Chemistry, 4032 Debrecen, Egyetem tér 1., Hungary, Tel. +36 52 412 345; Fax. +36 52 412 566, e-mail: baip@med.unideb.hu

Abstract

Our study aimed at finding a mechanistic relationship between the gut microbiome and breast cancer. Breast cancer cells are not in direct contact with these microbes, but disease could be influenced by bacterial metabolites including secondary bile acids that are exclusively synthesized by the microbiome and known to enter the human circulation. In murine and bench experiments, a secondary bile acid, lithocholic acid (LCA), reduced cancer cell proliferation (by 10-20%) and VEGF production (by 37%), aggressiveness and metastatic potential of primary tumors through inducing mesenchymal-to-epithelial transition, increased antitumor immune response, OXPHOS and the TCA cyle. Part of these effects was due to activation of TGR5 by LCA. Early stage breast cancer patients, versus control women, had reduced serum LCA levels, reduced chenodeoxycholic acid to LCA ratio, and reduced abundance of the baiH (7α/β-hydroxysteroid dehydroxylase, the key enzyme in LCA generation) gene in fecal DNA, all suggesting reduced microbial generation of LCA in early breast cancer.

Keywords

breast cancer, lithocholic acid, endothelial-mesenchymal transition, OXPHOS, microbiome, TGR5

Highlights

- Lithocholic acid (LCA), is a secondary bile acid produced only by bacteria.
- LCA is cytostatic to breast cancer cells in vitro and in vivo in its serum reference range.
- LCA treatment induces OXPHOS and the TCA cyle, inhibits EMT, VEGF expression and boosts antitumor immunity.
- LCA expert its effects through the TGR5 receptor.
- In early stage breast cancer patients bacterial LCA production is reduced.

1. Introduction

The human body harbors a vast number of symbiotic, commensal and pathogenic bacteria in the bodily cavities and the body surface. The ensemble of these microbes is referred as the microbiota and its collective genome as the microbiome. Recent advances pointed out that changes in the composition of the microbiome and certain bacterial metabolites crucially impact metabolic, behavioral, cardiovascular and immune functions of the host and have pivotal roles in diseases that were previously not associated with bacteria [1-4]. Alterations of the microbiome are associated with certain cancers. Although, the microbiota may have a widespread role in carcinogenesis, the number of directly tumorigenic bacteria is extremely small, some 10 bacterial species fall into this category [5]. It seems more likely that pathological changes in the microbiota/microbiome (dysbiosis) determine susceptibility to the disease or influence the progression of the disease [4].

Most of these cancers affect those organs that are directly in contact with microbes such as the urinary tract [6], cervix [7], skin [8], airways [9], and the colon [4]. Such microbiome-host interactions are best characterized in the colon. In the intestine a breach of the biological barrier between the microbes and the underlying tissues enables an adverse physical contact between microbes and host cells, that induces the production of paracrine bacterial metabolites [4]. Through these, the microbiome modulates tumorigenesis, tumor promotion, severity of the disease, and chemotherapy effectiveness in colonic tumors [4]. Direct stimulation of the cancer cells by bacteria probably has role in bacteria-mediated induction of lymphomas [10, 11] and possibly prostate cancer [6].

Much less is known of the role of the microbiome in the regulation of those tumors that are located to different compartments and are indirectly connected to the microbiome through the circulation. Changes in the microbiome is associated with metabolic diseases (e.g. obesity or type II diabetes) [12]. These metabolic diseases are risk factors of certain cancers, among them, breast cancer [13, 14]. It is likely that similar mechanisms can confer susceptibility to cancer as to metabolic diseases. Blood-borne bacterial metabolites (e.g. short chain fatty acids) mediate human metabolism, hence these metabolites are likely candidates to be transported to a potential tumor by the bloodstream to exert carcinogenic or anti-carcinogenic effects in distant tumors. For hepatocellular carcinoma, lipopolysaccharide [15] and deoxycholic acid (DCA) [16] have been identified as promoters, while propionate, a short chain fatty acid (SCFA), is an inhibitor [17].

Numerous bacterial metabolites have been identified that are either the microbes' own metabolites (e.g., short chain fatty acids, lactate, pyruvate) or modified products of the host (e.g., secondary bile acids, metabolites of aromatic amino acids, redox-modified sex steroids) [18-20]. These bioactive metabolites act through various pathways that involve the modification of gene expression (e.g., activation of histone deacetylases and other lipid-

mediated transcription factors) or the modulation of signal transduction in the host. Our aim with the current study was to investigate a potential causal link between changes in the microbiome, microbiome-derived metabolites and breast cancer.

2. Materials and methods

2.1. Chemicals

All chemicals were from Sigma-Aldrich (St. Louis, MO, USA) unless otherwise stated.
Radioactively labelled substrates for the pulse-chase metabolomics experiment were from Cambridge Isotope Laboratories, Andover, MA, USA. The inhibitors and antagonists used in the TGR5 experiments (U73343 (phospholipase C inhibitor), NF449 ($G_{s\alpha}$-selective antagonist), CINPA1 (CAR antagonist), DY268 (FXR antagonist), GSK2033 (LXR antagonist)) were obtained from Tocris Bioscience and were used at the concentration of 5 µM except for U73343 which was used at a final concentration of 1 µM.

2.2. Image based correlation spectroscopy (ImFCS)

After an exponential of polynomial bleach correction, pixel-by-pixel autocorrelation functions (ACFs) were calculated using a multi-tau correlation scheme [21]. To obtain the diffusion coefficient (D) for all pixels ACFs were fitted according to the equation in [21]. To identify and describe the mode of membrane organization by investigating the size-dependency of diffusion coefficient, we used the Imaging FCS type of FCS diffusion law [22]. According to that, the diffusion time (τ_D) of the fluorescent probe depends on the observation area (A_{eff}), as described by

$$\tau_D(A_{eff}) = \tau_0 + \frac{A_{eff}}{D}$$

where A_{eff} is the area of the membrane in which the labeled particle travels across,τ_0 is the intercept of the diffusion law plot on the y-axis of A_{eff}/D vs. A_{eff}. This parameter provides information about the diffusion confinement. A more detailed description of the method can be found among the Supplementary Materials.

2.3. Cell culture

MCF7 cells were maintained in MEM (Sigma-Aldrich) medium supplemented with 10 % FBS, 1 % penicillin/streptomycin and 2 mM L-glutamine at 37 °C with 5 % CO_2.
4T1 cells were maintained in RPMI-1640 (Sigma-Aldrich) medium containing 10 % FBS and 1 % penicillin/streptomycin, 2 mM L-glutamine and 1 % pyruvate at 37 °C with 5 % CO_2.

SKBR3 cells were maintained in DMEM (Sigma-Aldrich, 1000 mg/l glucose) medium supplemented with 10 % FBS, 1 % penicillin/streptomycin and 2 mM L-glutamine at 37 °C with 5 % CO_2.

Primary fibroblasts cells were maintained in DMEM (Sigma-Aldrich, 1000 mg/l glucose) medium supplemeted with 20 % FBS, 1 % penicillin/streptomycin, 2 mM L-glutamine and 10 mM HEPES at 37 °C with 5 % CO_2.

2.4. In vitro cell proliferation assays

Sulphorhodamine B assays were described in [23]. For colony formation assays five hundred cells were seeded in a 6-well plate in complete medium and were cultured with the indicated concentrations of LCA for 7 days. At the end of the assay plates were washed twice in PBS. Colonies were fixed in methanol for 15 minutes, dried and stained according to May-Grünwald-Giemsa for 15 minutes. Plate was washed with water and the colonies were counted using Image J software [24].

2.5. Detection of cell death

LCA-induced cytotoxicity was determined by propidium iodide (PI) uptake. Cells were seeded in 6-well plate (MCF7 - 200.000 cell/well; 4T1 - 75.000 cell/well) treated with LCA for two days and stained with 100 µg/ml propidium iodide for 30 min at 37 °C, washed once in PBS, and analyzed by flow cytometry (FACSCalibur, BD Biosciences).

2.6. Scratch assay and video microscopy

Cells were grown in 6-well plates until cell confluence reached about 70-80 %. The plates were manually scratched with sterile 200 µl pipette tip, followed by washing the cells twice with PBS. Then cells were incubated with vehicle or LCA (0.3 µM) in a thermostate. Cell densities were monitored every hour for one day using JuLi Br Live cell movie analyzer (NanoEnTek Inc., Seoul, Korea).

2.7. Electric Cell-substrate Impedance Sensing (ECIS)

ECIS (Electric cell-substrate impedance sensing) model Zθ, Applied BioPhysics Inc. (Troy, NY, USA) was used to monitor transcellular electric resistance of MCF7 and 4T1 cells seeded (MCF7- 40.000 cell/well; 4T1- 20.000 cell/well) on type 8W10E arrays. Cell were treated with vehicle or 0.3 µM LCA after 20 hours and total impedance values were measured for additional 48 hours. Multifrequency measurements were taken at 62.5, 125, 250, 500, 1000, 2000, 4000, 8000, 16000, 32000, 64000 Hz. Modeling tool of ECIS was used to evaluate the Rb (barrier resistance) values of each of the wells at fix 180 s interval. The reference well was set to a no-cell control with complete medium.

2.8. DNA and mRNA preparation and quantitation; EMT screen

DNA was extracted from fecal samples using PowerSoil DNA Isolation kit (*MO BIO* Laboratories, Inc. Carlsbad, California) according to the manufacturer's instructions.

Total RNA from cells and tumor samples were prepared using TRIzol reagent (Invitrogen Corporation, Carlsbad, CA).

For the assessment of the expression of individual genes two micrograms of RNA were reverse transcribed using High Capacity cDNA Reverse Transcription Kit (Applied Biosystems, Foster City, CA, USA). The qPCR reactions were performed with qPCRBIO SyGreen Lo-ROX Supermix (PCR Biosystems Ltd, London, UK) on Light-Cycler 480 Detection System (Roche Applied Science). Geometric mean of 36B4 and cyclophyllin was used for normalization. Primers are listed in **Table 1**.

For the assessement of the abundance of the baiH ORF 10 ng of DNA (from fecal samples) was used for qPCR reactions. Primers are listed in **Table 2**. Specificity of the qPCR reactions were verified by sequencing PCR products with the primers used for the amplification.

2.9. Metabolomics, pulse-chase metabolomics

Cells, grown in the presence of LCA, were harvested after 48 hours of treatment. After quenching in liquid nitrogen the labelled (in D5030 medium for 1 hour were with 10 mM [U-^{13}C]-glucose or [2-^{13}C]-acetate - Cambridge Isotope Laboratories, Andover, MA, USA) and unlabeled cells were extracted in methanol–chloroform–H_2O solution at 4 °C. The supernatant was separated by centrifugation (15 000 g for 10 min at 4 °C) and stored at −80 °C till further analysis. Drying and sonicating samples in 3-nitrobenzyl alcohol-trimethyl-chlorosilane solution followed 80 °C incubation. The reaction was stopped by adding ammonium bicarbonate. The samples were diluted with acetonitril-water solution and the derivate metabolites were separated by reversed-phase chromatography in Waters Acquity LC system. For the measurements Waters Micromass Quattro Micro triple quadrupole mass spectrometer (Waters Corporation, Milford MA, USA) was operated with an electrospray source in positive ion mode.

2.10. Measurement of oxygen consumption and extracellular acidification rate

Oxygen consumption rate (OCR) and changes in pH, extracellular acidification rate (ECAR) were measured using an XF96 oxymeter (Seahorse Biosciences, North Billerica, MA, USA). Cells were seeded in 96-well Seahorse assay plate (MCF7 - 3000 cells/well; 4T1 - 1500 cells/well) and treated with vehicle and LCA for two days. Then oxygen consumption was recorded every 30 minutes to follow the LCA effect. Data were normalized to protein content.

2.11. SDS-PAGE and Western blotting

Cells were lysed in RIPA buffer (50 mM Tris, 150 mM NaCl, 0.1 % SDS, 1 % TritonX 100, 0.5 % sodium deoxycolate, 1 mM EDTA, 1 mM Na_3VO_4, 1 mM NaF, 1 mM PMSF, protease inhibitor coctail). Protein extracts were separated on 10% SDS polyacrylamide gels and transferred onto nitrocellulose membranes by electroblotting. Membranes were blocked with 5 % BSA, and incubated with primary antibodies for overnight at 4 °C. The membranes were washed with 1X TBS-TWEEN and probed with IgG HRP conjugated secondary antibodies (Cell Signaling Technology, Inc. Beverly, MA, 1:2000). Bands were visualized by enhanced chemiluminescence reaction (SuperSignal West Pico Solutions, Thermo Fisher Scientific Inc, Rockford, USA). Antibodies used in this study are listed in **Table 3**.

2.12. Immunocytochemistry

Cells were grown on coverslips, washed with PBS, fixed with 4 % paraformaldehyde for 15 minutes and permeabilized using 1 % Triton X-100 for 5 minutes. Then cells were blocked with 1 % BSA for one hour and incubated with TexasRed-X Phalloidin (Invitrogen, Oregon, USA) for 45 minutes for the analysis of cellular morphology. Typical mesenchymal-like morphology and epithelial-like morphology of MCF7 and 4T1 cells are represented on **Fig. S3**.

For cellular localization of NRF1 protein cells were incubated overnight with NRF1 primary antibody at 4 °C. After washing steps, cells were incubated with secondary antibody (1:600, anti-rabbit Alexa 488, Life technologies) for 1 hour at room temperature. Cell nuclei were visualized with TO-PRO-3 iodide (1:1000, Life technologies). Coverslips were rinsed and mounted in Mowiol/Dabco solution. Confocal images were acquired with Leica SP8 confocal microscope and LAS AF v3.1.3 software.

2.13. Transfections

Silencer Select siRNA targeting TGR5 (GPBAR1- cat.no. 4392420; siRNA ID: s195791), VDR cat.no. 4390824; siRNA ID: s14777) and Negative control siRNA #1 (cat.no. 4390843) were obtained from Thermo Fisher Scientific. Cells were seeded in 24-well plate (MCF7 - 50.000 cell/well) and on next day cells were transfected with TGR5, VDR siRNA and negative control at a final concentration of 30 nM using Lipofectamine RNAiMAX transfection reagent (Invitrogen). Cells were incubated with transfection complexes in medium containing LCA (0.3 μM) for 48 h.

2.14. Animal study

All animal experiments were authorized by the local and national ethical board (reg. 1/2015/DEMÁB) and were performed to conform the relevant EU and US guidelines.

Experimental animals were female BALB/c animals between 8-10 weeks of age (20-25 g). Mice were randomized for all experiments animals were. Animals were bred in the “specific pathogen free” zone of the Animal Facility at the University of Debrecen, and kept in the “minimal disease” disease zone during the experiment. Animal studies are reported in compliance with the ARRIVE guidelines.

No more than six mice were housed in each cage (standard block shape 365 × 207 × 140 mm, surface 530 cm^2; 1284 L Eurostandard Type II. L from Techniplast) with Lignocel Select Fine (J. Rettenmaier und Söhne, Germany) as bedding. Mice had paper tubes to enrich their environment. Dark/light cycle was 12 h, and temperature 22 ± 1°C. Cages were changed once a week, on the same day. Mice had ad libitum access to food and water (sterilized tap water). The animal facility was overseen by a veterinarian. A total of 28 mice was used in this study, group sizes are indicated in the figure captions.

2.14.1. 4T1 tumor injection

4T1 cells were suspended ($2x10^6$/mL) in ice cold PBS-matrigel (1:1, Sigma-Aldrich) at 1:1 ratio. From this suspension female BALB/c mice received 50 µL injections to their 2^{nd} inguinal fat pads on both sides (10^5 cells/injection). Tumor growth and animal wellbeing was monitored daily.

2.14.2. LCA treatment

Animals received daily oral LCA treatments. LCA stock was prepared in 96% ethanol at 100x concentration (7.5 mM) for storage at -20°C. LCA stock was diluted each day to a working concentration of 75 µM in sterile PBS immediately before the treatment. Ethanol vehicle (1% in PBS) was prepared and diluted similarly. Animals received a daily oral dose of 200 µL/30 g bodyweight from the LCA solution or the vehicle. Researchers administering LCA and vehicle solutions were blinded. Treatment was administered every day at the same time during the morning hours between 8am and 10am.

2.14.3. Infiltration score

During autopsy tumors were visually assessed and scored based on their infiltration rate into surrounding tissues. If the tumor mass remained in the mammary fat pads without any detectable attachment to muscle tissues then it was classified as a “low infiltration” tumor. In case the tumor mass attached to the muscle tissue below the fat pad but hasn’t penetrated it then it was classified as a “medium infiltration” tumor. Finally, if the tumor mass grew into the muscle tissue and penetrated the abdominal wall then it was scored a “high infiltration” tumor. Researchers involved in scoring primary tumors for their infiltration rate were blinded.

2.14.4. TIL calculation

Tumor infiltrating lymphocytes (TIL) content of tumors was expressed as the number of TILs per 100 tumor cells.

2.15. Human studies

The study in which human feces samples were collected from healthy subjects and breast cancer patients was developed by collaborators at the National Cancer Institute (NCI), Kaiser Permanente Colorado (KPCO), the Institute for Genome Sciences at the University of Maryland School of Medicine, and RTI International. The study protocol and all study materials were approved by the Institutional Review Boards at KPCO, NCI, and RTI International (IRB number 11CN235).

The study in which human serum samples were collected from healthy subjects and breast cancer patients was developed by collaborators at the University of Debrecen (Hungary). The study protocol and all study materials were approved by the Institutional and Hungarian Review Boards (3140-2010).

Cohort for fecal DNA and serum studies are listed in **Table 4**.

2.15.1. Serum bile acid determination

Serum bile acid profile was assessed as in [25].

2.16. Database search

The kmplot.com database was used to study the link between gene expression levels and breast cancer survival in humans. The association of known mutations with breast cancer was retrieved from www.intogen.org/. Gene expression profiles were retrieved from the Gene expression omnibus (www.ncbi.nlm.nih.gov/geoprofiles/). The sequence of the *baiH* ORF or the *bai* operon was retrieved from the KEGG (www.genome.jp/kegg/) and the PATRIC databases (www.patricbrc.org/).

2.17. Statistical analysis

We used two tailed Student's *t*-test for the comparison of two groups unless stated otherwise. Fold data were $\log_2$ transformed to achieve normal distribution. For multiple comparisons one-way analysis of variance test (ANOVA) was used followed by Tukey's honestly significance (HSD) post-hoc test. Data is presented as average ± SD unless stated otherwise, percent changes are listed in **Table 5**. Outliers were identified for Fig. S3B using the Thomson tau-test. Statistical analysis was done using GraphPad Prism VI software.

3. Results

3.1. Lithocholic acid attenuates the aggressiveness of experimental breast cancer

Primary bile acids are converted to secondary bile acids exclusively by the intestinal microbiota [26]. Therefore, changes elicited by secondary bile acids directly implicate the involvement of the intestinal microbiota. We investigated three secondary bile acids, lithocholic acid (LCA), deoxycholic acid (DCA) and ursodeoxycholic acid (UDCA) in concentrations corresponding to their normal (reference) concentrations in human serum and breast tissue (10 nM – 10 μM) [19, 27] first in short term proliferation assays. LCA reduced cellular proliferation of MCF7, SKBR3 and 4T1 breast cancer cells but did not affect primary fibroblasts (10 nM – 10 μM) (**Fig. 1A, Table 5**). Other secondary bile acids such as DCA or UDCA were without effect on MCF7 and 4T1 breast cancer cells (**Fig. 1B**). In the subsequent assays we used LCA concentrations higher than the reference serum concentration of LCA (~30-50 μM) as higher LCA concentrations (100-1000 nM) were reported in the breast [27]. The cytostatic effect of LCA was verified in longer colony forming assays (**Fig. 1C, Table 5**). The percent of propidium-iodide positive cells did not change upon LCA treatment suggesting that LCA did not induce cell death (**Fig. 1D**).

We tested the cytostatic property of LCA in mice that were grafted with 4T1 cells and were treated with LCA (15 nmol LCA p.o. q.d.) or vehicle for 18 days. At the time of the sacrifice the infiltration capacity of the primary tumor to the surrounding tissues markedly decreased upon LCA treatment (**Fig. 2A**). Furthermore, the number of the metastases was also lower in the LCA-treated group (**Fig. 2B**).

3.2. LCA interferes with multiple anticancer molecular pathways

After finding the cytostatic property of LCA in breast cancer, we investigated how LCA modulates the different features of breast cancer through assessing classical hallmarks of cancer [28].

LCA inhibited tumor infiltration and metastasis formation (**Fig. 2A-B**), implicating modulation of the epithelial-mesenchymal transition (EMT) and cellular movement. LCA treatment improved cell-to-cell connections, an epithelial feature, as reflected by epithelial-like morphology in cells (**Fig. 3A, Fig. S3A**) and improved total impedance (**Fig. 3B, Table 5**) that provide functional evidence of better cell-to-surface and cell-to-cell adhesion. LCA-treatment inhibited β-catenin signaling as evidenced by lower GSK-3α and GSK-3β phosphorylation and lower β-catenin protein content both in cell lines and *in vivo* (**Fig. 3C, Fig. S3B**). Furthermore, LCA-treated 4T1 cells were slower in moving into a void area in a scratch assay as compared to vehicle-treated ones (**Fig. 3D**). In addition, we found lower VEGF mRNA expression (**Fig. 3E, Table 5**) and higher number of tumor infiltrating lymphocytes (TILs) in LCA-treated as compared to vehicle-treated ones mice (TILs) (**Fig. 3F**).

Breast cancer depends on Warburg metabolism [29]. Therefore, we assessed LCA-induced changes in cellular metabolism. LCA treatment induced glycolysis (extracellular acidification rate - ECAR) and mitochondrial respiration (oxygen consumption rate - OCR) levels (**Fig. 4A**). In line with that, intracellular lactate and citrate levels, as well as, citrate/lactate ratio increased upon LCA treatment (**Fig. 4B**). In line with these observations, LCA-induced the expression of a set of OXPHOS genes in 4T1 and MCF7 cells (**Fig. 4C, Table 5**).

Next, we performed pulse-chase metabolomics experiments in MCF7 and 4T1 cells treated with 300 nM LCA. When cells were charged with ^{13}C-acetate, a metabolite that can fuel the TCA cycle, LCA treatment enhanced the incorporation of ^{13}C into succinate and malate (**Fig. 4D**) suggesting increased flux through the TCA cycle. Next, we fed cells with ^{13}C-glucose from which ^{13}C atoms must enter glycolysis to subsequently feed the TCA cycle or form lactate. LCA treatment enhanced the amount of ^{13}C-labelled citrate and lactate in MCF7 cells and the amount of ^{13}C-labelled succinate and lactate in 4T1 cells (**Fig. 4E**). In line with these observations, the ratio between ^{13}C-citrate and ^{13}C-lactate or between ^{13}C-succinate and ^{13}C-lactate increased, providing further evidence towards mitochondrial dominance of the LCA-induced metabolic switch (**Fig. 4E**). We assessed the distribution of ^{13}C-labelled carbons in citrate in vehicle and LCA-treated MCF7 cells. More carbons were ^{13}C-labelled in citrate in the LCA-treated cells as compared to vehicle treated ones (**Fig. S4**) suggesting a more rapid turning of the TCA cycle. Taken together, LCA treatment induced the TCA cycle and oxidative phosphorylation (OXPHOS) in breast cancer cells.

We assessed components of the cellular energy sensor web and mitochondrial transcriptional regulators to find the roots of the above metabolic changes. LCA-induced expression and activation of positive regulators of mitochondrial oxidative phosphorylation *FOXO1, PGC-1β* and nuclear respiratory factor-1 (NRF1) (**Fig. 5A, Fig S5A**). LCA not only boosted their expression but also enhanced their activation that is evidenced by enhanced nuclear translocation of NRF1 and the higher phosphorylation of ACC (**Fig. 5A, B, Fig S5A, C**). In the *in vivo* experiments we also observed the LCA-mediated induction of AMPK activity (marked by increased phospho-ACC and phospho-AMPK levels) and enhanced expression of FOXO1 as well, although neither NRF1, nor PGC-1β expression was induced by LCA (**Fig. 5C, Fig S5B**).

Subsequently, we assessed whether the induction of the metabolic regulators (NRF1, AMPK, PGCs) have (patho)physiological relevance in humans. Previous studies have underlined the antitumor activity of AMPK and FOXO1 in humans [23, 30, 31]. Using the kmplot.com database we found that high expression of NRF1 in breast cancer tissue is predictive of better survival post-diagnosis (**Fig. 5D**). Although no frequent (driver) mutations were found in PGC-1β according to the Intogen database, it did appear that the expression of

PGC-1β was reduced in tumor as compared to healthy tissues [32, 33] and in metastases as compared to the primary tumors [34]. Taken together, the modulation of AMPK, FOXO1, PGC-1β or NRF1 may have (patho)physiological relevance in modulating LCA-evoked effects in humans.

Next, we aimed to identify the LCA receptor(s) responsible for the above effects. We used pharmacological inhibitors designed to inhibit different LCA receptors (see Materials and methods) to test their involvement in the LCA-induced effects. MCF7 cells were treated with LCA together with vehicle or pharmacological agents blocking the potential LCA receptors. LCA-mediated reduction in cell proliferation was efficiently blocked by CINPA1, NF449 and U73343; other inhibitors were ineffective (**Fig. 6A, Table 5**). NF449 and U73343, unlike CINPA1, efficiently blocked LCA-induced morphological changes (closure of the void areas among cells, epithelial-like morphology) in MCF7 and 4T1 cells (**Fig. 6B**). Since NF449 and U73343 are not TGR5-specific inhibitors but block TGR5 signaling, by inhibiting Gsα and phospholipase C, we transiently silenced TGR5 in MCF7 cells (**Fig. 6C, D, Fig. S6A, Table 5**) to provide direct evidence for the involvement of TGR5. Silencing of TGR5 efficiently blocked LCA-induced morphological changes (**Fig. 6E**) and blocked the LCA-induced increases in the mRNA expression of *CYTOCHROME C, ATP5G1* and *NDUFB5* mitochondrial markers (**Fig 6F, Table 5**) and markers of AMPK activation (**Fig. 6G, Fig. S6B**). Silencing of VDR receptor had no effect on LCA- induced changes (data not shown). It is also of note that LCA, in the concentrations used in this study, enters biomembranes but does not alter either its dynamical properties or microdomain organization, since neither the diffusion constant (D), nor the confinement time (TD) changed even upon 100 μM LCA treatment (**Fig. 6H**).

3.3. LCA biosynthesis is suppressed in early phases of human breast cancer

We next investigated how bile acid and LCA metabolism relates to breast cancer in humans. LCA is produced through deconjugation of chenodeoxycholic acid (CDCA) conjugates, followed by a dehydroxylation on carbon 7 by the action of the enzyme 7α/β hydroxysteroid dehydrogenase (7-HSDH) [26] that is the rate-limiting step of LCA formation. The enzymes involved in the 7-dehydroxylation of bile acids are organized into one operon called the bile acid-inducible (*bai*) operon wherein the *baiH* ORF codes for 7-HSDH in most bacterial species [26].

baiH abundance was assessed by amplifying *baiH* ORF from fecal DNA using specific primers. To validate this mode of measurement, we treated mice with ciprofloxacin (CPX), an antibiotic that specifically kills aerobic bacteria, while leaving the anaerobic bacteria intact. When mice were treated with CPX (200 mg/kg q.d. for two weeks) the abundance of *staphylococcal*, *escherichial* and *pseudomonal baiH* (aerobic bacteria) decreased, while the

ratio of the *baiH* of the anaerobic bacteria (*Bacteroides fragilis, Clostridium scindens*) did not change (**Fig. 7**), as expected from the biology of the antibiotic that supports this approach.

Total bile acid, CDCA and LCA levels were reduced in serum from breast cancer patients as compared to age and sex matched healthy individuals (**Fig. 8A, B, C, Table 6**), and we observed a similar trend in all other bile acids we examined (**Fig. 8A, Table 6**). Since both primary and secondary bile acid levels were lower in breast cancer patients, we assessed the ratio between CDCA (the substrate for LCA synthesis) and LCA in human serum. We found a decrease in the LCA/CDCA ratio in breast cancer patients compared to healthy individuals, and this decrease that was more marked when only stage 1 patients were assessed (**Fig. 8D**). At later stages LCA/CDCA ratio normalized and even increased above the ratio of healthy individuals in stage 3 patients. These data are in good correlation with the data of Tang an co-workers [35] demonstrating that glycolithocholate sulphate levels were lower in breast cancer patients compared to controls (additional file 3, line 239).

To get an insight how intestinal LCA biosynthesis is altered in breast cancer patients, we assessed the abundance of the *baiH* ORF in human fecal DNA from the experimental cohort described in [36] (Table 4, cohort 2). In order to do that we searched for bacterial species where the ORF for baiH was annotated. We identified the baiH ORF of anaerobic, Gram positive and Gram negative species and measured the abundance of the baiH DNA in fecal DNA samples using qPCR assays. When all patients were compared to healthy controls the abundance of baiH of *Clostridium sordelli, Staphylococcus haemolyticus, Escherichia coli* and *Pseudomonas putida* was lower in breast cancer patients (**Fig. 8E**) in line with the lower LCA levels and LCA/CDCA ratio. A more pronounced decrease in the abundance of the baiH of *Bacteroides thetaiotaomicron, Clostridium sordelli, Staphylococcus haemolyticus, Escherichia coli* and *Pseudomonas putida* were observed in stage 0 and stage 1 patients than in the pool of all patients (**Fig. 8F**).

Taken together, the bacterial LCA biosynthesis machinery in the intestine is downregulated in breast cancer patients that is very pronounced in the early phase of the disease. Lower capacity to synthesize LCA then contributes to lower LCA levels. These findings together with the observation of Tang and co-workers [35] that glycolithocholate sulphate levels have a significant negative correlation with Ki67 positivity (additional file 9, line 110) in human breast cancer tumors, pointing towards the involvement of bacterial LCA metabolism in human breast cancer pathogenesis.

4. Discussion

This study nominates LCA, a metabolite of the microbiota, to be synthesized in the gut and thereafter transferred through the bloodstream to the breast where it may be an important player in bringing about an anti-cancer tumor microenvironment. In our studies

LCA inhibited the proliferation of breast cancer cells, while it did not interfere with primary cells. In previous studies [37, 38] LCA induced cell death in neuroblastoma, prostate cancer, and MCF7 cells. However, the LCA concentrations utilized in those studies [37, 38] were higher than the one used in our present study, which may explain why we did not observe acute LCA toxicity. As we noted earlier, 100-1000 nM LCA concentration, used in this study, stands closer to the LCA concentrations reported in the breast [27].

To date no direct, causal relationship had been shown between the microbiome and breast cancer, although studies have suggested an interconnection. Specifically, the gut microbiome had been suggested to facilitate breast cancer progression through deconjugating estrogens making them more prone for reuptake [36, 39]. Goedert and co-workers [36] have assessed microbiome changes in breast cancer patients, finding that postmenopausal breast cancer patients had reduced diversity and altered composition of the gut microbiome compared to closely matched control women. In addition, bacteria were identified on breast duct surfaces, and differences in the microbiome of breast cancer tissue has also been observed [14, 40-42]. These findings suggest that LCA may be produced by the breast's own microbiota and not only by the gut microbiome. However, the share of the two sources (breast vs. gut) in LCA production is not known.

A causative relationship between the microbiome and breast cancer is further strengthened by the suggestive association between antibiotic treatment and incidence or recurrence of breast cancer [43-48]. Although the chance of uncontrolled confounding is high and some studies have found no association, evidence for a dose-response relationship between antibiotic exposures and breast cancer incidence has been found [43, 44, 46-48]. The correlation between antibiotic use and breast cancer incidence was also found in males [48]. The cancer association has not been tied to a particular antibiotic class, but the strongest correlations have been with tetracyclins and macrolids [45]. These observations support our hypothesis on the relationship between microbiota functions and breast cancer.

Which bacterial species are important in LCA-mediated modulation of breast cancer? This question is hard to answer at the moment. Goedert and colleagues [36] found that in the gut microbiota breast cancer cases had increased relative abundance of *Clostridiaceae*, *Faecalibacterium*, and *Ruminococcaceae* and decreased *Dorea* and *Lachnospiraceae* taxa. In contrast to that, previous studies showed that anaerobic microbes are instrumental in the production of secondary bile acids, such as LCA [26]. In our study, hereby, we demonstrated decreases in both the aerobic and the anaerobic microbial populations with early stage breast cancer suggesting widespread suppression of the microflora in breast cancer that culminates in decreased LCA production. These imply the contribution of the aerobic flora in LCA synthesis.

Hereby, we demonstrate the antiproliferative effects of LCA against breast cancer cells. In contrast to that, previous studies have pointed out possible oncogenic properties to secondary bile acid [20]. LCA was shown to possess transforming capacity towards colon epithelial cells [20], while DCA, that is inactive in our model systems, was shown to reprogram hepatocyte secretome and through that promote hepatocellular carcinoma [16, 49]. Bile acids also are implicated in pharyngeal cancer [50]. The explanation for these differences are yet unknown.

To our best knowledge, this is the first study that provides mechanistic evidence of crosstalk between the microbiome and breast cancer by describing LCA as a bacterial metabolite with antiproliferative effects in breast cancer. It is very likely that other bacterial metabolites that can increase or, like LCA, inhibit the proliferation of breast cancer cells will be described in the future. The fact that the composition of the microbiome influences breast cancer may provide novel approaches to cancer risk estimation and prevention.

5. Conclusions

In this study we show that a bacterial metabolite, lithocholic acid, can limit the proliferation of breast cancer cells *in vitro* and *in vivo* through activating TGR5 receptor, furthermore, in early stages of breast cancer LCA biosynthesis and LCA levels drop suggesting a role for this pathway in human disease.

List of abbreviations

ACC - Acetyl-CoA Carboxylase
AMPK - AMP -Activate Kinase
ATP5g1 - ATP Synthase, H+Transporting, Mitochondrial Fo Complex Subunit C1 (Subunit 9)
bai operon - bile acid-inducible operon
CDCA - chenodeoxycholic acid
CPX - ciprofloxacin
CYTC - Cytochrome C, Somatic (CYCS)
DCA - deoxycholic acid
ECAR - extracellular acidification rate
ECIS - Electric Cell-substrate *Impedance* Sensing
EMT - epithelial-mesenchymal transition
FOXO1 - Forkhead Box O1
LCA - lithocholic acid
ImFCS - Image based correlation spectroscopy
NDUFB5 - NADH Dehydrogenase (Ubiquinone) 1 Beta Subcomplex, 5
NRF1 - Nuclear Respiratory Factor-1

OCR - oxygen consumption rate
OXPHOS – Oxidative phosphorylation
PGC-1β - Peroxisome Proliferator-Activated Receptor Gamma Coactivator 1 Beta
PI - propidium iodide
SRB assay - Sulphorhodamine B assay
TGR5/GPBAR1 - G Protein-Coupled Bile Acid Receptor 1
TIL - tumor infiltrating lymphocytes
UDCA - ursodeoxycholic acid
VEGFA - Vascular Endothelial Growth Factor A
7-HSDH - 7α/β hydroxysteroid dehydrogenase

Data availability

Primary data created in relation with the current study is available at https://figshare.com/s/66407d07fe82b289c1bd. The dataset will become freely available upon the acceptance of the manuscript.

Acknowledgments

We are grateful for Mr. László Finta for the technical assistance and to Dr. Beáta Lontay (Dept. Medical Chemistry, UD) for enabling us the use of the JuLi Br real-time videomicroscope. The authors are also thankful to Dr. Jacques Ravel (University of Maryland Medical School) for transferring the human fecal specimens to Dr. László Takács (BSI KFT., Debrecen, Hungary) for the human serum specimens, to Dr. Viktor Dombrádi (Dept. Medical Chemistry, UD) and Dr. Balint L. Balint (Dept. of Biochemistry and Molecular Biology, UD) for the valuable discussions.

Our work was supported by grants from NKFIH (K123975, PD116262, PD124110, GINOP-2.3.2-15-2016-00006, GINOP-2.3.3-15-2016-00021), the Momentum fellowship of the Hungarian Academy of Sciences and the University of Debrecen and a Bolyai fellowship to GT, AS and AB. This work was supported by the Intramural Research Program of the National Cancer Institute at the National Institutes of Health (Z01CP010214).

Conflict of interest statement

The authors have no competing financial or non-financial interests to declare.

Authors' contributions

Metabolomics: ZH, AS; Histological examination: TC, GM; ECIS: AB; Cellular experiments: EM, TK, GU, JM, ZS, PK; Animal study: AV, GT; Human fecal specimens: JJG; Human serum samples: ASP; Determination of serum bile acids: MW; Membrane biology

experiments: IG, LV; Statistical analysis: EM, AV; Wrote the manuscript: PB, JS, GM, AS, JJG, BC

References

1. Reijnders, D, et al., *Effects of Gut Microbiota Manipulation by Antibiotics on Host Metabolism in Obese Humans: A Randomized Double-Blind Placebo-Controlled Trial.* Cell Metab., 2016. **24**(1): p. 63-74.
2. Smits, LP, et al., *Therapeutic potential of fecal microbiota transplantation.* Gastroenterology, 2013. **145**(5): p. 946-53.
3. Krishnan, S, N Alden, and K Lee, *Pathways and functions of gut microbiota metabolism impacting host physiology.* Curr Opin Biotechnol., 2015. **36**: p. 137-45.
4. Garrett, WS, *Cancer and the microbiota.* Science, 2015. **348**(6230): p. 80-6.
5. de Martel, C, et al., *Global burden of cancers attributable to infections in 2008: a review and synthetic analysis.* Lancet Oncol., 2012. **13**(6): p. 607-15.
6. Yu, H, et al., *Urinary microbiota in patients with prostate cancer and benign prostatic hyperplasia.* Arch Med Sci, 2015. **11**(2): p. 385-94.
7. Chase, D, et al., *The vaginal and gastrointestinal microbiomes in gynecologic cancers: a review of applications in etiology, symptoms and treatment.* Gynecol Oncol, 2015. **138**(1): p. 190-200.
8. Yu, Y, et al., *The role of the cutaneous microbiome in skin cancer: lessons learned from the gut.* J Drugs Dermatol, 2015. **14**(5): p. 461-5.
9. Gui, QF, et al., *Well-balanced commensal microbiota contributes to anti-cancer response in a lung cancer mouse model.* Genet Mol Res, 2015. **14**(2): p. 5642-51.
10. Yamamoto, ML and RH Schiestl, *Lymphoma caused by intestinal microbiota.* Int J Environ Res Public Health, 2014. **11**(9): p. 9038-49.
11. Yamamoto, ML and RH Schiestl, *Intestinal microbiome and lymphoma development.* Cancer J., 2014. **20**(3): p. 190-4. .
12. Kahn, SE, ME Cooper, and S Del Prato, *Pathophysiology and treatment of type 2 diabetes: perspectives on the past, present, and future.* Lancet, 2013. **3**(13): p. 62154-6.
13. Sundaram, S, AR Johnson, and L Makowski, *Obesity, metabolism and the microenvironment: Links to cancer.* J Carcinog, 2013. **12**(19): p. 19.
14. Xuan, C, et al., *Microbial dysbiosis is associated with human breast cancer.* PLoS One., 2014. **9**(1): p. e83744. .
15. Dapito, DH, et al., *Promotion of hepatocellular carcinoma by the intestinal microbiota and TLR4.* Cancer Cell, 2012. **21**(4): p. 504-16.
16. Yoshimoto, S, et al., *Obesity-induced gut microbial metabolite promotes liver cancer through senescence secretome.* Nature., 2013. **499**(7456): p. 97-101.
17. Bindels, LB, et al., *Gut microbiota-derived propionate reduces cancer cell proliferation in the liver.* Br J Cancer, 2012. **107**(8): p. 1337-44.
18. Wikoff, WR, et al., *Metabolomics analysis reveals large effects of gut microflora on mammalian blood metabolites.* Proc Natl Acad Sci U S A, 2009. **106**(10): p. 3698-703.
19. Smith, JL, et al., *Endogenous ursodeoxycholic acid and cholic acid in liver disease due to cystic fibrosis.* Hepatology, 2004. **39**(6): p. 1673-82.
20. Rowland, IR, *The role of the gut flora in toxicity and cancer*. 1988, Carshalton, UK: Academic press.
21. Sankaran, J, et al., *ImFCS: a software for imaging FCS data analysis and visualization.* Opt Express., 2010. **18**(25): p. 25468-81.
22. Ng, XW, N Bag, and T Wohland, *Characterization of Lipid and Cell Membrane Organization by the Fluorescence Correlation Spectroscopy Diffusion Law.* Chimia (Aarau), 2015. **69**(3): p. 112-9.

23. Fodor, T, et al., *Combined Treatment of MCF-7 Cells with AICAR and Methotrexate, Arrests Cell Cycle and Reverses Warburg Metabolism through AMP-Activated Protein Kinase (AMPK) and FOXO1.* PLoS One., 2016. **11**(2): p. e0150232.
24. Rueden, CT, et al., *ImageJ2: ImageJ for the next generation of scientific image data.* BMC Bioinformatics., 2017. **18**(1): p. 529.
25. Watanabe, M, et al., *Bile acids induce energy expenditure by promoting intracellular thyroid hormone activation.* Nature., 2006. **439**(7075): p. 484-489.
26. Ridlon, JM, DJ Kang, and PB Hylemon, *Bile salt biotransformations by human intestinal bacteria.* J Lipid Res, 2006. **47**(2): p. 241-59.
27. Raju, U, M Levitz, and NB Javitt, *Bile acids in human breast cyst fluid: the identification of lithocholic acid.* J Clin Endocrinol Metab., 1990. **70**(4): p. 1030-4.
28. Hanahan, D and RA Weinberg, *Hallmarks of cancer: the next generation.* Cell, 2011. **144**(5): p. 646-74.
29. Giguère, V, et al., *Functional domains of the human glucocorticoid receptor.* Cell, 1986. **46**(5): p. 645-652.
30. Hardie, DG, *Molecular Pathways: Is AMPK a Friend or a Foe in Cancer?* Clin Cancer Res., 2015. **21**(17): p. 3836-40.
31. Cheng, J, et al., *Prognostic significance of AMPK in human malignancies: A meta-analysis.* Oncotarget., 2016. **7**(46): p. 75739-75748. .
32. PPARGC1B - Ductal carcinoma in situ: mammary gland. Date accessed: 2017. 11. 27. https://www.ncbi.nlm.nih.gov/geoprofiles/70231836
33. Pregnancy-associated breast cancer: laser capture microdissected epithelia and stroma. Date accessed: 2017. 11. 27. https://www.ncbi.nlm.nih.gov/geo/tools/profileGraph.cgi?ID=GDS4766:232181_at
34. Ppargc1b - Human Epidermal Growth Factor Receptor 2-positive breast cancer MMTV-Her2/Neu murine model: primary and secondary mammary tumors. Date accessed: 2017. 11. 27. https://www.ncbi.nlm.nih.gov/geoprofiles/78744132
35. Tang, X, et al., *A joint analysis of metabolomics and genetics of breast cancer.* Breast Cancer Res, 2014. **16**(4): p. 415.
36. Goedert, JJ, et al., *Investigation of the association between the fecal microbiota and breast cancer in postmenopausal women: a population-based case-control pilot study.* J Natl Cancer Inst, 2015. **107**(8): p. djv147.
37. Goldberg, AA, et al., *Lithocholic bile acid selectively kills neuroblastoma cells, while sparing normal neuronal cells.* Oncotarget., 2011. **2**(10): p. 761-82.
38. Goldberg, AA, et al., *Bile acids induce apoptosis selectively in androgen-dependent and -independent prostate cancer cells.* PeerJ., 2013. **1**(doi): p. e122.
39. Plottel, CS and MJ Blaser, *Microbiome and malignancy.* Cell Host Microbe, 2011. **10**(4): p. 324-35.
40. Hieken, TJ, et al., *The Microbiome of Aseptically Collected Human Breast Tissue in Benign and Malignant Disease.* Sci Rep., 2016. **6**: p. 30751.

survivors. Sci Rep., 2016. **6**: p. 28061.

42. Urbaniak, C, et al., *The Microbiota of Breast Tissue and Its Association with Breast Cancer.* Appl Environ Microbiol., 2016. **82**(16): p. 5039-48.
43. Velicer, CM, et al., *Antibiotic use in relation to the risk of breast cancer.* JAMA., 2004. **291**(7): p. 827-35.
44. Velicer, CM, et al., *Association between antibiotic use prior to breast cancer diagnosis and breast tumour characteristics (United States).* Cancer Causes Control., 2006. **17**(3): p. 307-13.
45. Friedman, GD, et al., *Antibiotics and risk of breast cancer: up to 9 years of follow-up of 2.1 million women.* Cancer Epidemiol Biomarkers Prev., 2006. **15**(11): p. 2102-6.
46. Wirtz, HS, et al., *Frequent antibiotic use and second breast cancer events.* Cancer Epidemiol Biomarkers Prev., 2013. **22**(9): p. 1588-99. .

47. Tamim, HM, et al., *Risk of breast cancer in relation to antibiotic use.* Pharmacoepidemiol Drug Saf., 2008. **17**(2): p. 144-50.
48. Satram-Hoang, S, et al., *A pilot study of male breast cancer in the Veterans Affairs healthcare system.* J Environ Pathol Toxicol Oncol, 2010. **29**(3): p. 235-44.
49. Xie, G, et al., *Dysregulated hepatic bile acids collaboratively promote liver carcinogenesis.* Int J Cancer., 2016. **139**(8): p. 1764-75. doi: 10.1002/ijc.30219. Epub 2016 Jun 17.
50. Shellman, Z, et al., *Bile acids: a potential role in the pathogenesis of pharyngeal malignancy.* Clin Otolaryngol., 2017. **42**(5): p. 969-973.
51. Howlader, N, et al., *Overview of breast cancer collaborative stage data items--their definitions, quality, usage, and clinical implications: a review of SEER data for 2004-2010.* Cancer., 2014. **120**(Suppl 23): p. 3771-80.

Figure legends

Figure 1. LCA inhibits the proliferation of breast cancer cells

(A) MCF7, 4T1, SKBR3 cells and primary fibroblasts were treated with LCA in the concentrations indicated for 48 hours then total protein concentration was determined in SRB assays (MCF7: n=8; 4T1: n=6; SKBR3: n=3; fibroblasts n=5). Values expressed as fold changes, where 1 means protein content in the control cells and is marked by a dotted line. **(B)** MCF7 and 4T1 cells were treated with DCA or UDCA in the concentrations indicated for 48 hours then total protein concentration was determined in SRB assays (MCF7: n=4; 4T1: n=3). **(C)** MCF7 and 4T1 cells were treated with LCA in the concentrations indicated for 7 days and colonies were stained according to May-Grünwald-Giemsa that were then counted using the Image J software (MCF7: n=3, 4T1: n=4). **(D)** MCF7 and 4T1 cells were treated with LCA in the concentrations indicated for 48 hours. Dead cells were stained by propidium iodide (PI) and analyzed by flow cytometry (MCF7, 4T1: n=3).

* and ** indicate statistically significant difference between vehicle and treated groups at $p<0.05$ or $p<0.01$, respectively.

Figure 2. LCA supplementation reduces cancer aggressiveness *in vivo*

(**A-B**) Female Balb/c mice were grafted with 4T1 cells as described and were treated with LCA (15 nmol q.d. p.o.) or vehicle (VEH) (n=8/8) for 18 days before sacrifice. Upon autopsy (A) tumor infiltration was scored and (B) the number of metastases were determined.

On panel A significance was calculated using the Freeman-Halton extension of the Fisher exact probability test for a 2x3 contingency table. * indicate statistically significant difference between vehicle and treated groups at $p<0.05$. Error is shown as SEM.

Figure 3. LCA treatment reverses EMT and improves antitumor immune response

A part of the experiments were performed on MCF7 and 4T1 cells treated with LCA in the concentrations indicated for 48 hours, or on female Balb/c mice grafted with 4T1 cells that were treated with LCA (15 nmol q.d. p.o.) or vehicle (VEH) (n=8/8) for 18 days.

(A-B) In LCA or VEH-treated MCF7 and 4T1 cells (A) cellular morphology was assessed after Texas Red-X Phallodin- and To-Pro-3 staining (representative figure, n=3), (B) total resistance was measured in ECIS experiments (mean ± SD, n=3). **(C)** In LCA-treated 4T1 and MCF7 cells, as well as in tumor samples the expression of the indicated proteins were analyzed by Western blotting (MCF7, 4T1 n=3, representative figures throughout). **(D)** Scratch assays were performed on 4T1 cells (n=3). **(E)** VEGF expression was determined in tumors using RT-qPCR (mean marked by a line). **(F)** The morphology in LCA or VEH-treated tumors were assessed in hematoxilin-eosine stained 4 µm thick histological sections and the number of tumor infiltrating lymphocytes (mean marked by a line) was counted in the sections. The relative numbers of TILs were determined according to the recent diagnostic procedure by counting both the tumor cells and the intratumor lymphocytes within the same representative areas of the HE stained slides. TIL counts were given in relation to tumor cell count in percentage. Stars mark typical tumor cells, TILs are marked by arrows. Scale bar on panel (A) is 10 µm and 50 µm on panel (F).

*, ** and *** indicate statistically significant difference between vehicle and treated groups at $p<0.05$, $p<0.01$ or $p<0.001$ respectively. Abbreviations are in the text.

Figure 4. LCA treatment induces the TCA cycle and OXPHOS in breast cancer cells

(A-E) MCF7 and 4T1 cells were treated with LCA in the concentrations indicated for 48 hours then the indicated measurements were performed. (A) Extracellular acidification rate (ECAR) (average± SD of a representative measurement, n=2) and oxygen consumption rate (OCR) (average±SD of a representative measurement, n=2) were performed and data were plotted. (B) Intracellular lactate levels (MCF7, 4T1: n=2) and citrate levels were determined (MCF7, 4T1: n=2) and were plotted. **(C)** The expression of a set of genes were determined in RT-qPCR reactions (MCF7 n=3, 4T1 n=2; error is depicted as SEM). **(D)** MCF7 and 4T1 cells were treated with LCA in the concentrations indicated for 48 hours then cells were loaded with 10 mM ^{13}C-acetate for 1 hour that was followed by the determination of the indicated metabolites. **(E)** MCF7 and 4T1 cells were treated with LCA in the concentrations indicated for 48 hours then cells were loaded with 10 mM ^{13}C-glucose for 1 hour that was followed by the determination of the indicated metabolites.

* indicate statistically significant difference between citrate or OCR values of vehicle and treated groups at $p<0.05$. # or ## indicate statistically significant difference between lactate or ECAR values of vehicle and treated groups at $p<0.05$ or $p<0.01$, respectively.

Figure 5. LCA treatment induces elements of the energy stress sensors

(A) MCF7 and 4T1 cells were treated with LCA in the concentrations indicated for 48 hours then protein extracts were separated by PAGE, blotted onto nitrocellulose and probed with the antibodies indicated. (MCF7, 4T1: n=3) **(B)** NRF1 localization was assessed by immunofluorescence and image analysis. Scale bar equals to 50 µm. **(C)** Female Balb/c mice were grafted with 4T1 cells were treated with LCA (15 nmol q.d. p.o.) or vehicle (VEH) for 18 days. Protein, extracted from the primary tumors, was separated by PAGE, blotted onto nitrocellulose and probed with the antibodies indicated. **(D)** The impact of NRF1 expression on survival in breast cancer was evaluated by assessing the kmplot.com database.

Abbreviations are in the text. ** and *** indicate statistically significant difference between vehicle and treated groups at $p<0.01$ or $p<0.001$, respectively.

Figure 6. LCA-evoked anticancer effects are partly mediated by TGR5

(A) MCF7 cells were treated with 0.3 µM LCA and the agents as follows: 5 µM NF449, 1 µM U73343, 5 µM CINPA1, 5 µM DY268 and 5 µM GSK2033 for 48 hours, then cellular proliferation was determined (n=3). **(B)** MCF7 and 4T1 cells (n=3) were treated with 0.3 µM LCA and the agents as follows: 5 µM NF449, 1 µM U73343 and 5 µM CINPA1 for 48 hours, then actin was stained with Texas-Red-X-phalloidin. Arrows point at void areas around cells and lost focal adhesion sites. Scale bar equals to 25 µm. **(C-D)** TGR5 was silenced in MCF7 cells by transiently transfecting an siRNA or a negative control, non-specific siRNA to the cells for 48 hours, then (C) mRNA and (D) protein expression of TGR5 was determined. **(E-G)** TGR5 depleted and negative control-transfected MCF7 cells were treated with 0.3 µM LCA for 48 hours. (E) Cells were stained with Texas-Red-X-phalloidin. Arrows point at void areas around cells and lost focal adhesion sites. Scale bar equals to 25 µm. The (F) mRNA expression of the indicated genes were determined by RT-qPCR, while (G) the expression levels of the indicated proteins were determined by Western blotting.

(H) Supported bilayer with ternary lipid composition of DOPC/SM/cholesterol in 1/1/1 ratio was treated with 100 µM LCA for 20 minutes. Diffusion coefficients of STAR 488 PEG-cholesterol probe in control and treated membranes. Confinement times of the probe in control and treated membranes. Error bars represent the standard deviations (n=6). Please note that the LCA concentration was 33 times higher than the highest concentration applied in *in vivo* or *in vitro* experiments.

* and ** indicate statistically significant difference between vehicle and treated groups at $p<0.05$ or $p<0.01$ respectively.

Figure 7. Ciprofloxacin treatment alters the abundance of baiH DNA

Balb/c female mice were grafted with 10^6 4T1 cells. Feces was collected before grafting and 18 days post grafting. Fecal DNA was isolated and the abundance of the baiH ORF of the bacterial species indicated on the figure was assessed in these samples in qPCR reactions. Abbreviations are in the text. ** indicates statistically significant difference between vehicle and treated groups at $p<0.01$.

Figure 8. In early stages of human breast cancer bacterial LCA biosynthesis is suppressed

(A-D) Serum samples from the healthy controls and breast cancer patients of cohort 1 were pooled. (A) The bile acid composition of these pooled samples were determined. (B) By summing the different bile acid species total serum bile acid content was calculated. (C) Serum CDCA and LCA levels from the samples of healthy controls and breast cancer patients are plotted. (D) LCA/CDCA ratio was calculated from the samples of healthy controls and breast cancer patients. **(E-F)** The abundance of the baiH DNA was determined in the fecal DNA samples of cohort 2 (median values indicated by a line). Values where c_t was lower than 45 were removed. Panel E depicts only the comparison of the control vs. cases, therefore, on that panel Student's t-test was used to determine statistical significance.

* and ** indicate statistically significant difference at $p<0.05$ and $p<0.01$ between the groups indicated, respectively.

Table 1. Primers used in the RT-qPCR reactions

Gene Symbol	Murine forward and reverse primer (5'-3')	Human forward and reverse primer (5'-3')
Atp5g1	GCTGCTTGAGAGATGGGTTC AGTTGGTGTGGCTGGATCA	CTAAACAGCCTTCCTACAGCAACTT TGAACCAGCCACACCAACTGT
Ndufb5	CTTCGAACTTCCTGCTCCTT GGCCCTGAAAAGAACTACG	GTATTCATTGGTCAAGCTGAACTAG CAGCTCCTTTACCCGTAATTCAGC
Cytc	TCCATCAGGGTATCCTCTCC GGAGGCAAGCATAAGACTGG	TAAGAACAAAGGCATCATCTGG AGGCAGTGGCCAATTATTACTC
36b4	AGATTCGGGATATGCTGTTGG AAAGCCTGGAAGAAGGAGGTC	CCATTGAAATCCTGAGTGATGTG GTCGAACACCTGCTGGATGAC
Cyclophilin	TGGAGAGCACCAAGACAGACA TGCCGGAGTCGACAATGAT	GTCTCCTTTGAGCTGTTTGCAGAC CTTGCCACCAGTGCCATTATG

Table 2. Primers used for the determination of baiH abundance using qPCR.

	Forward primer (5'-3')	**Reverse primer (5'-3')**
Bacteroides fragilis	CGGGCAGATCGATGTACTGGT	AGTACCATTCGAATCGGCCGT
Bacteroides thetaiotaomicron	CCCATCATGACCACTCACGGA	AAGAACCAGTCCCGGTGCTAC
Escherichia coli	TATGGCGTTTGACCTGGGTGA	CAAAGGAACAGCGCTGCGTTA
Clostridium scindens	GATGAGCTGGAGACCACCCTG	GTAGCCGTAGTCTCGCTGTCA
Clostridium sordelli	TGCCATACTCCTGAAATCGAGT	TCCCATCTTTCTTCAAATGTACGCT
Staphylococcus haemolyticus	CGTTTCTGTCGTGATAATGCCCT	GGCGTGTTTGAATGGTCGCTT
Pseudomonas putida	GGGCGATGCACTGGACTTCTA	ATGTGGGTGTTGTCCTCGAGG

Table 3. Antibodies used in the study

antibody/die	concentration	vendor
Phospho-ACC (Ser79)	1/1000	Cell Signaling Technology (#3661)
Phospho-AMPKα (Thr172)	1/1000	Cell Signaling Technology(#2531)
NRF1	1/1000 (WB) 1/100 (immunocytochemistry)	Abcam (ab175932)
PGC1β	1/1000	Abcam (ab176328)
FOXO1	1/1000	Cell Signaling Technology (#9454)
Phospho-GSK-3α/β (Ser21/9) (D17D2)	1/2000	Cell Signaling Technology (#8566)
GSK-3α/β (D75D3)	1/2000	Cell Signaling Technology (#5676)
β-Catenin	1/1000	Sigma (C7082)
TGR5/GPBAR1	1/1000	NOVUS (NBP2-23669)
TexasRed-X Phalloidin	1/150	Life Technologies (T7471)
ACTIN	1/20000	Sigma-Aldrich (A3854)

Table 4. Patient cohorts

Cohort for serum studies- cohort 1

	healthy	patient	of which				
			stage 0	stage 1	stage 2	stage 3	stage 4
number	56	56	-	16	25	10	5
age (years)	59.1±7.3	60.7± 8	-	61.8 ± 5,5	61.5 ± 8,6	60.6 ± 8,2	53.8 ± 10
sex	female	female	female	female	female	female	female

Patients were recruited at the Medical Center of the University of Debrecen. Patients were age and sex-matched with the staging was according to [51]. Patients with other cancers, inflammatory diseases, diseases affecting the GI tract and the liver or receiving antibiotics were excluded from the study.

Cohort for fecal DNA studies – cohort 2

	healthy	patient	of which Stage				
			stage 0	stage 1	stage 2	stage 3	stage 4
number	48	46	11	23	10	2	-
sex	female	female	female	female	female	female	-

This cohort was published in [36]. Staging of the patients was performed according to [51].

Table 5. Primary data expressed as percent change for Fig 1A, 1C, 3C, 3E, 4C, 6A, 6B, 6C, 6F

		LCA concentrations (μM)													
		CTL		0.1		0.3		1							
		AVG	SD	AVG	SD	AVG	SD	AVG	SD						
Fig1A	MCF7	**100,00**	0,00	**83,52**	8,95	**85,81**	5,57	**85,68**	8,87						
	4T1	**100,00**	0,00	**91,88**	6,67	**92,25**	3,99	**92,24**	5,16						
	SKBR	**100,00**	0,00	**88,59**	2,73	**87,20**	3,32	**88,14**	4,32						
		CTL		0.1		0.3		1							
		AVG	SD	AVG	SD	AVG	SD	AVG	SD						
Fig1C	MCF7	**100,00**	0,00	**89,22**	14,31	**75,72**	3,40	**80,75**	1,65						
	4T1	**100,00**	0,00	**74,15**	18,04	**81,25**	14,51	**63,85**	11,99						
		CTL						LCA (0.3 μM)							
		0		24h		48h		0		24h		48h			
		AVG	SD	AVG	SD	AVG	SD	AVG	SD	AVG	SD	AVG	SD		
Fig3B	MCF7	**100,00**	0,00	**118,38**	4,83	**119,46**	10,16	**100,00**	0,00	**135,35**	2,00	**129,44**	2,81		
	4T1	**100,00**	0,00	**202,94**	10,14	**287,53**	6,32	**100,00**	0,00	**238,75**	6,99	**371,71**	16,82		
		CTL		LCA											
		AVG	SD	AVG	SD										
Fig3E	in vivo/tumor	**100,00**	26,14	**63,91**	28,58										
		LCA concentrations (μM)													

		CTL		0.1		0.3		1							
		AVG	SEM	AVG	SEM	AVG	SEM	AVG	SEM						
Fig4 C	MCF7/CYTC	**100,00**	0,00	**121,00**	63,57	**201,00**	145,33	**191,67**	25,37						
	MCF7/ATP5G1	**100,00**	0,00	**184,00**	53,84	**308,50**	182,50	**143,67**	31,32						
	MCF7/NDUFB5	**100,00**	0,00	**168,33**	32,94	**225,25**	61,17	**151,75**	13,04						
	4T1/CYTC	**100,00**	0,00	**93,00**	4,51	**209,33**	95,25	**95,00**	2,00						
	4T1/ATP5G1	**100,00**	0,00	**119,00**	26,00	**138,00**	7,00	**109,00**	21,00						
	4T1/NDUFB5	**100,00**	0,00	**120,67**	14,24	**211,67**	32,67	**127,33**	26,03						
		CTL		LCA		NF449+LCA		U73343+LCA		CINPA1+LCA		DY268+LCA		GSK2033+LCA	
		AVG	SD	AVG	SD	AVG	SD	AVG	SD	AVG	SD	AVG	SD	AVG	SD
Fig6A	MCF7	**100,00**	0,00	**75,99**	9,95	**97,44**	11,18	**83,69**	10,15	**88,83**	12,92	**63,86**	10,88	**72,75**	9,74
		siNEG		siTGR5											
		AVG	SD	AVG	SD										
Fig6 C	MCF7	**100,00**	0,00	**42,06**	14,86										
		CTL		siNEG+LCA		siTGR5+LCA									
		AVG	SD	AVG	SD	AVG	SD								
Fig6F	MCF7/CYTC	**100,00**	0,00	**200,96**	9,11	**144,49**	44,62								
	MCF7/ATP5G1	**100,00**	0,00	**178,93**	8,26	**112,18**	53,39								

	MCF7/NDUFB5	**100,00**	0,00	**121,49**	7,58	**104,11**	30,04								

Table 6. Bile acid composition of the human serum samples (compare to Fig. 5 A-D)

Primary bile acids (µmol/L)

	CA	GCA	TCA	CDCA	GCDCA	TCDCA
Control	0,287	0,301	0,071	0,563	0,931	0,137
Breast cancer	0,116	0,166	0,033	0,262	0,761	0,173
Stage 1	0,170	0,126	0,020	0,342	0,591	0,078
Stage 2	0,092	0,177	0,043	0,198	0,874	0,263
Stage 3	0,113	0,170	0,033	0,205	0,710	0,150

Secondary bile acids (µmol/L)

	DCA	GDCA	TDCA	LCA	GLCA	UDCA	GUDCA
Control	0,701	0,415	0,061	0,031	0,025	0,147	0,330
Breast cancer	0,384	0,304	0,045	0,017	0,023	0,069	0,209
Stage 1	0,385	0,261	0,038	0,016	0,014	0,114	0,233
Stage 2	0,377	0,345	0,049	0,018	0,029	0,058	0,209
Stage 3	0,323	0,297	0,043	0,020	0,026	0,027	0,157

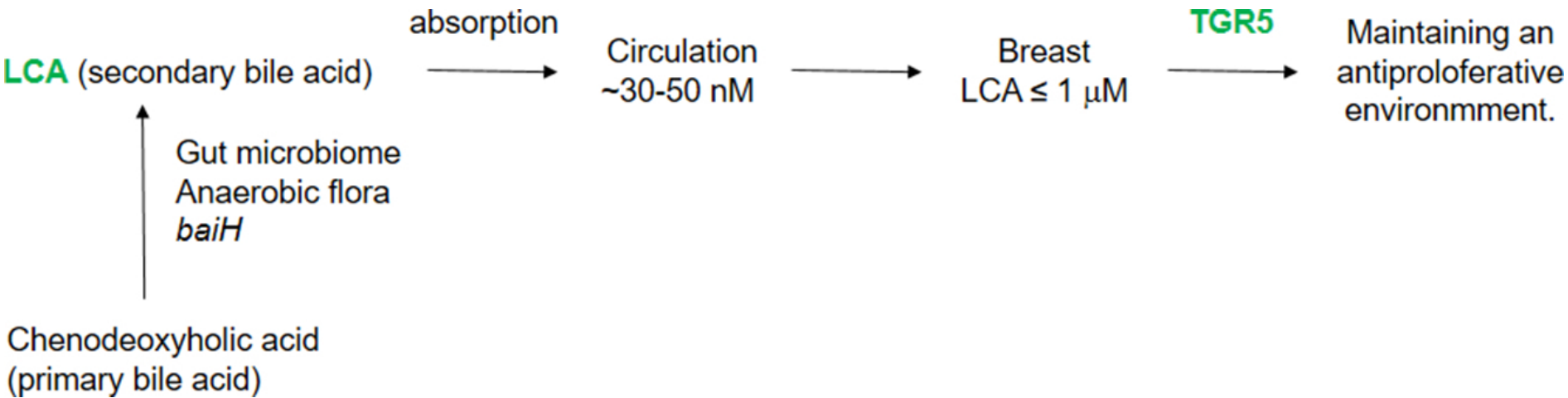

Graphics Abstract

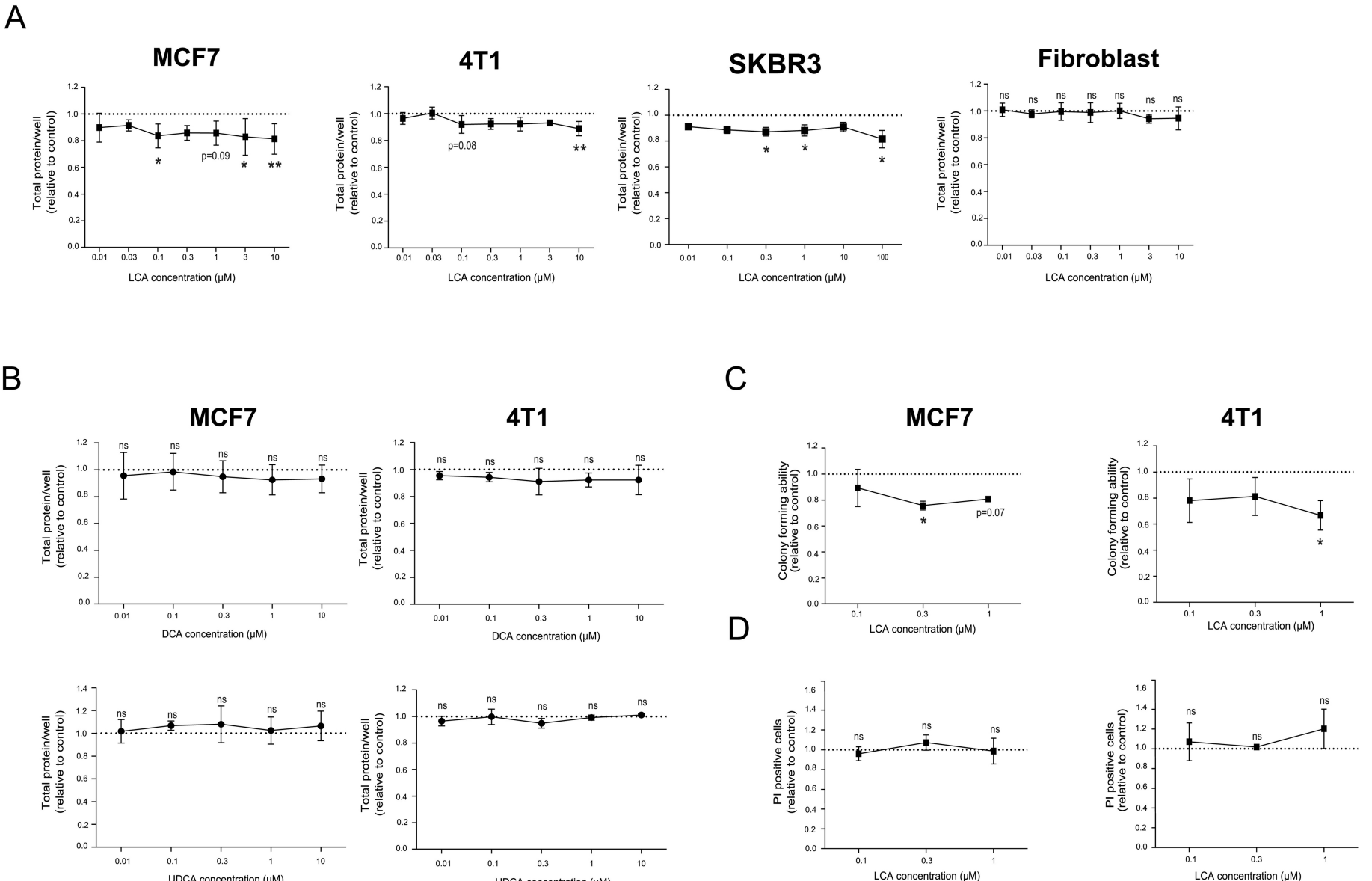
A
MCF7
4T1
SKBR3
Fibroblast
Total protein/well (relative to control)
LCA concentration (μM)
p=0.09
p=0.08
B
DCA concentration (μM)
UDCA concentration (μM)
C
Colony forming ability (relative to control)
p=0.07
D
PI positive cells (relative to control)
ns

Figure 1

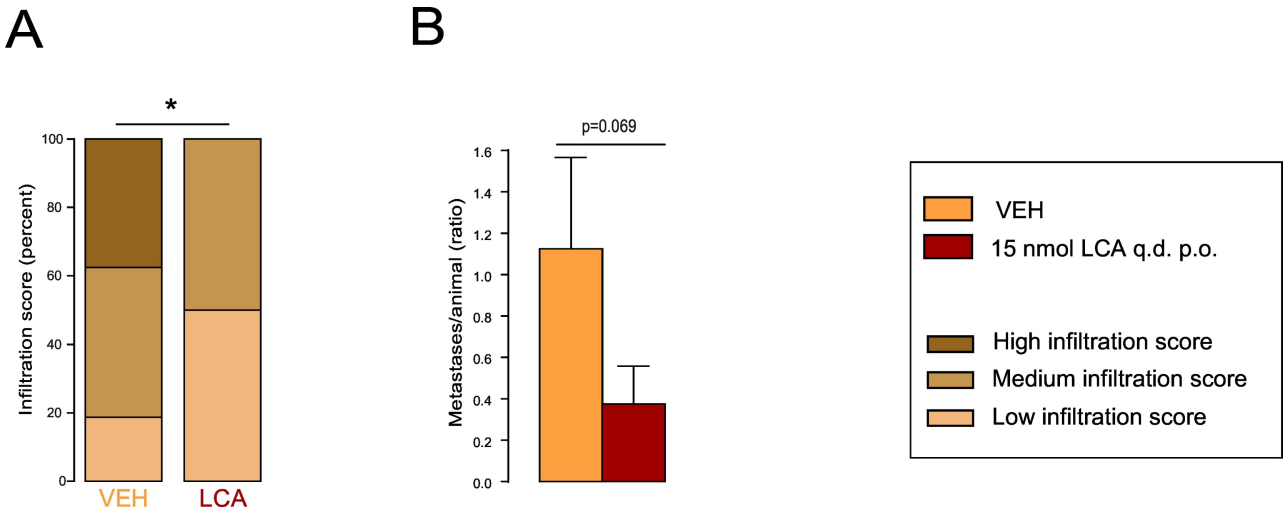
A
B
*
p=0.069
Infiltration score (percent)
Metastases/animal (ratio)
VEH
LCA
VEH
15 nmol LCA q.d. p.o.
High infiltration score
Medium infiltration score
Low infiltration score

Figure 2

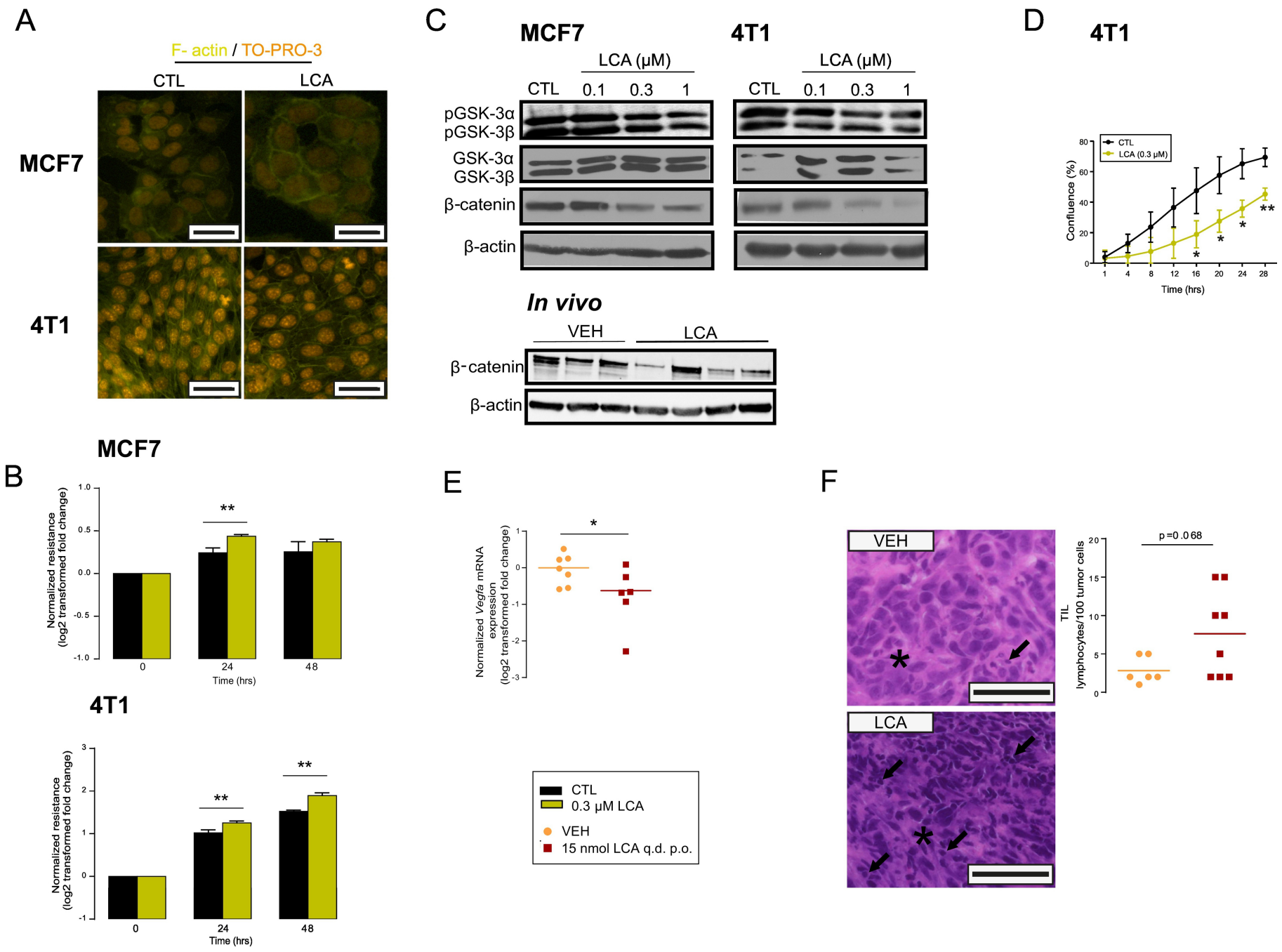
A
F- actin / TO-PRO-3
CTL
LCA
MCF7
4T1
B
MCF7
Normalized resistance (log2 transformed fold change)
Time (hrs)
4T1
C
MCF7
4T1
LCA (μM)
CTL
0.1
0.3
1
pGSK-3α
pGSK-3β
GSK-3α
GSK-3β
β-catenin
β-actin
In vivo
VEH
LCA
β-catenin
β-actin
D
4T1
Confluence (%)
CTL
LCA (0.3 μM)
Time (hrs)
E
Normalized Vegfa mRNA expression (log2 transformed fold change)
CTL
0.3 μM LCA
VEH
15 nmol LCA q.d. p.o.
F
VEH
LCA
TIL lymphocytes/100 tumor cells
p=0.068

Figure 3

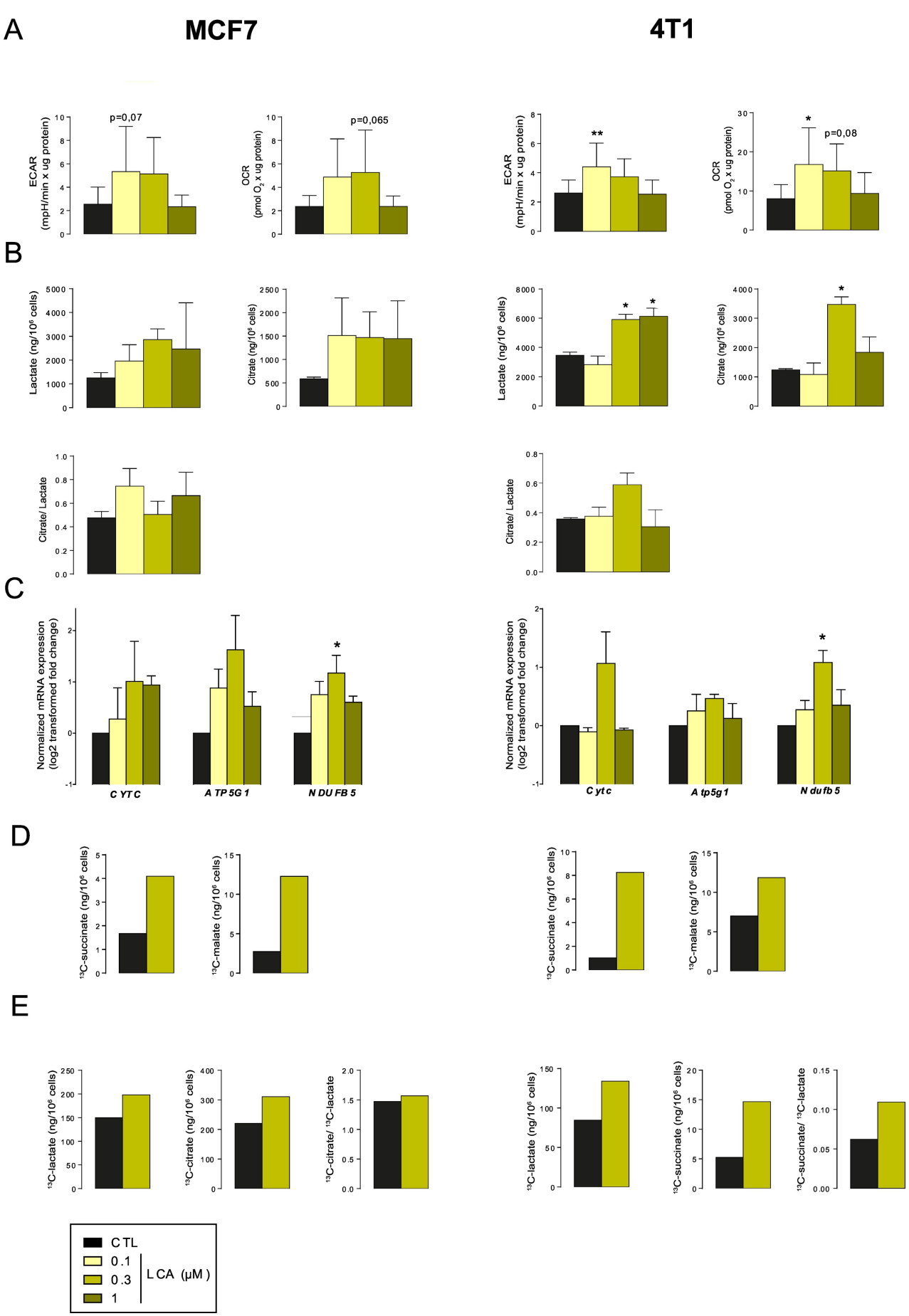
A
MCF7
4T1
ECAR (mpH/min x ug protein)
p=0,07
OCR (pmol O2 x ug protein)
p=0,065
**
*
p=0,08
B
Lactate (ng/10⁶ cells)
Citrate (ng/10⁶ cells)
Citrate/ Lactate
C
Normalized mRNA expression (log2 transformed fold change)
CYTC
ATP5G1
NDUFB5
Cytc
Atp5g1
Ndufb5
D
13C-succinate (ng/10⁶ cells)
13C-malate (ng/10⁶ cells)
E
13C-lactate (ng/10⁶ cells)
13C-citrate (ng/10⁶ cells)
13C-citrate/ 13C-lactate
13C-succinate (ng/10⁶ cells)
13C-succinate/ 13C-lactate
CTL
0.1
0.3
1
LCA (µM)

Figure 4

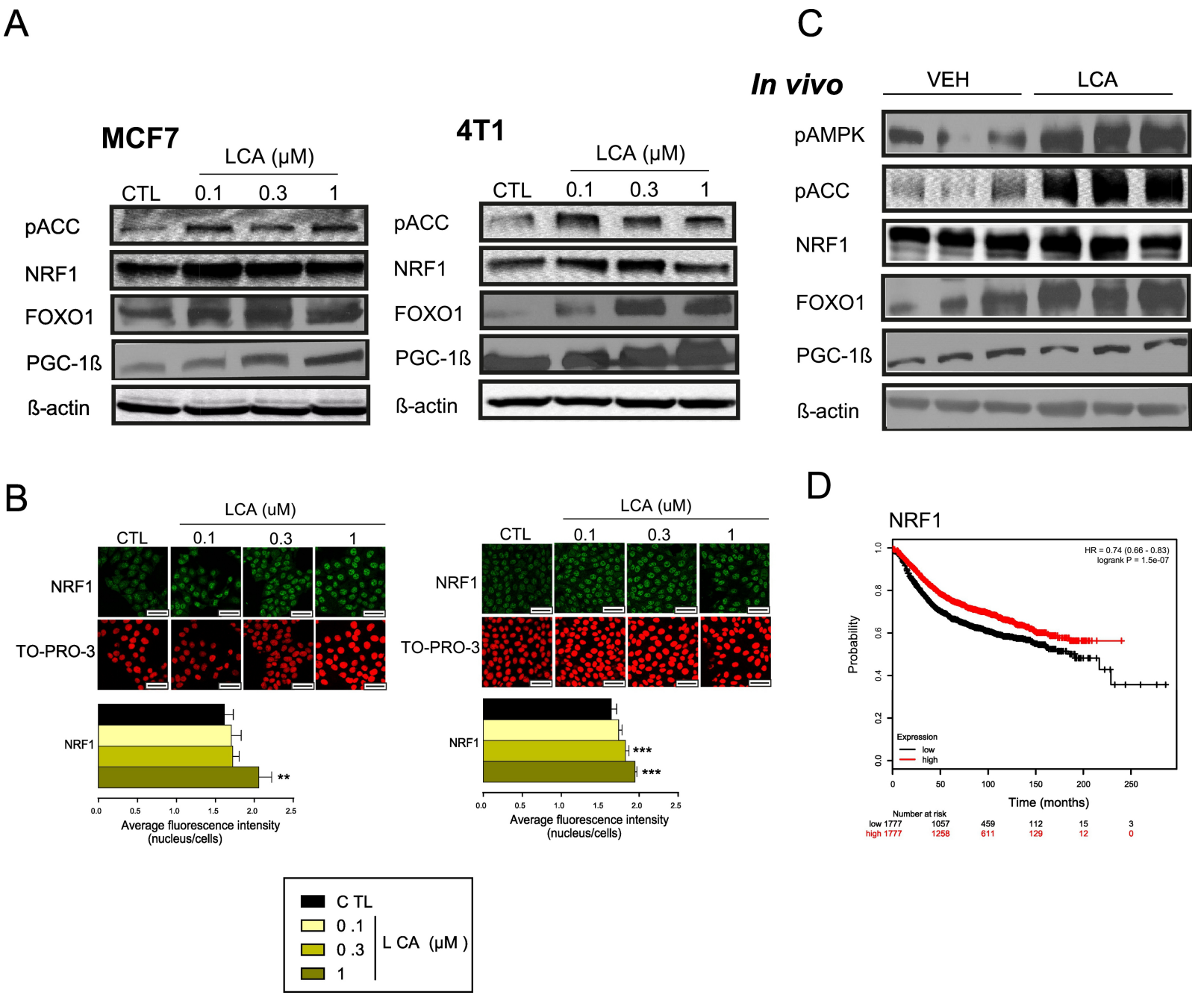
A
MCF7
LCA (μM)
CTL
0.1
0.3
1
pACC
NRF1
FOXO1
PGC-1ß
ß-actin
4T1
LCA (μM)
CTL
0.1
0.3
1
pACC
NRF1
FOXO1
PGC-1ß
ß-actin
C
In vivo
VEH
LCA
pAMPK
pACC
NRF1
FOXO1
PGC-1ß
ß-actin
B
LCA (uM)
CTL
0.1
0.3
1
NRF1
TO-PRO-3
NRF1
**
0.0
0.5
1.0
1.5
2.0
2.5
Average fluorescence intensity
(nucleus/cells)
LCA (uM)
CTL
0.1
0.3
1
NRF1
TO-PRO-3
NRF1
***
***
0.0
0.5
1.0
1.5
2.0
2.5
Average fluorescence intensity
(nucleus/cells)
C TL
0 .1
0 .3
1
L CA (μM)
D
NRF1
HR = 0.74 (0.66 - 0.83)
logrank P = 1.5e-07
Probability
0.0
0.2
0.4
0.6
0.8
1.0
Expression
low
high
0
50
100
150
200
250
Time (months)
Number at risk
low 1777 1057 459 112 15 3
high 1777 1258 611 129 12 0

Figure 5

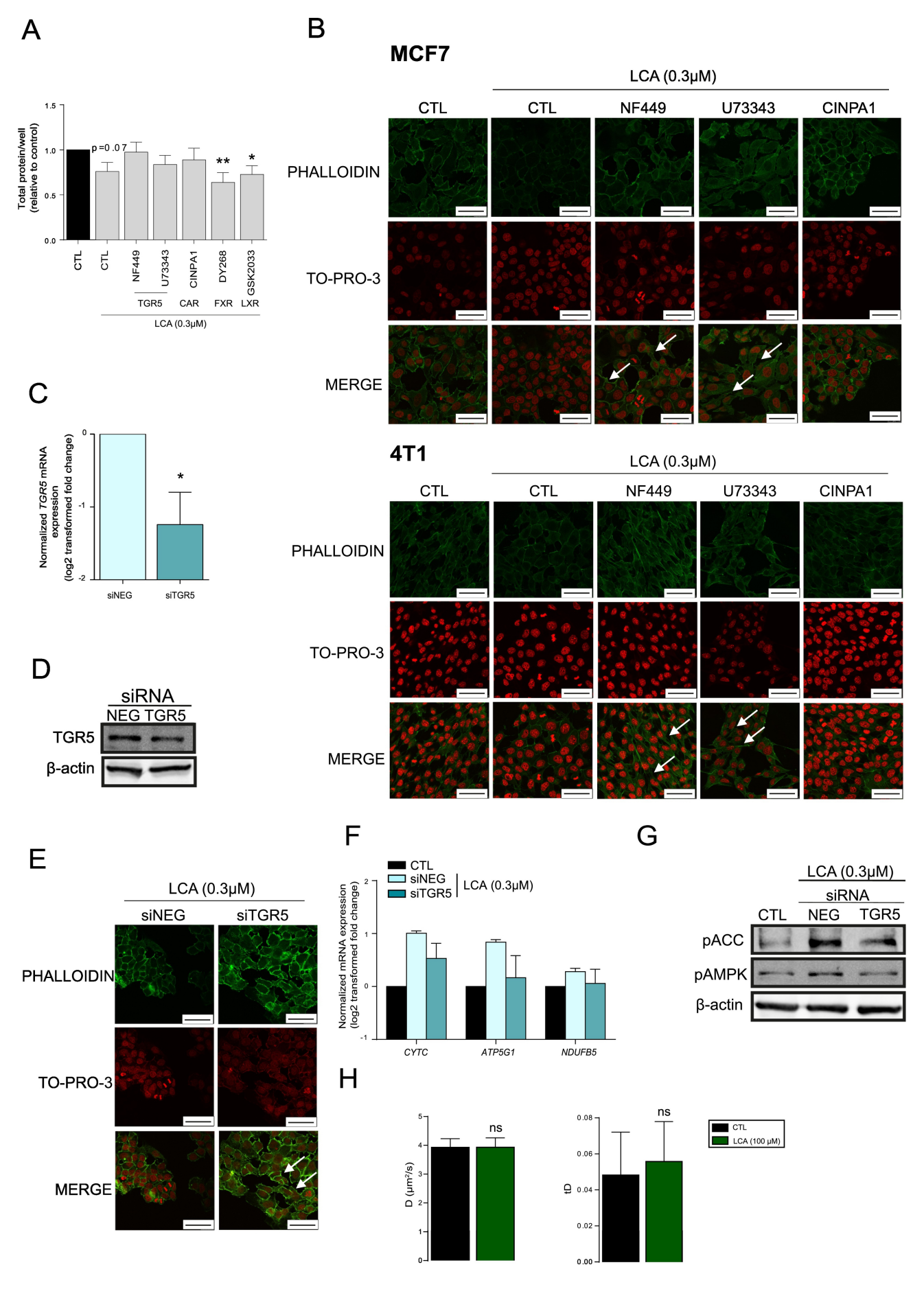
A
Total protein/well (relative to control)
p =0 .07
**
*
CTL
CTL
NF449
U73343
CINPA1
DY268
GSK2033
TGR5
CAR
FXR
LXR
LCA (0.3μM)
B
MCF7
LCA (0.3μM)
CTL
CTL
NF449
U73343
CINPA1
PHALLOIDIN
TO-PRO-3
MERGE
4T1
LCA (0.3μM)
CTL
CTL
NF449
U73343
CINPA1
PHALLOIDIN
TO-PRO-3
MERGE
C
Normalized TGR5 mRNA expression (log2 transformed fold change)
*
siNEG
siTGR5
D
siRNA
NEG TGR5
TGR5
β-actin
E
LCA (0.3μM)
siNEG
siTGR5
PHALLOIDIN
TO-PRO-3
MERGE
F
CTL
siNEG
siTGR5
LCA (0.3μM)
Normalized mRNA expression (log2 transformed fold change)
CYTC
ATP5G1
NDUFB5
G
LCA (0.3μM)
siRNA
CTL
NEG
TGR5
pACC
pAMPK
β-actin
H
D (μm²/s)
ns
tD
ns
CTL
LCA (100 μM)

Figure 6

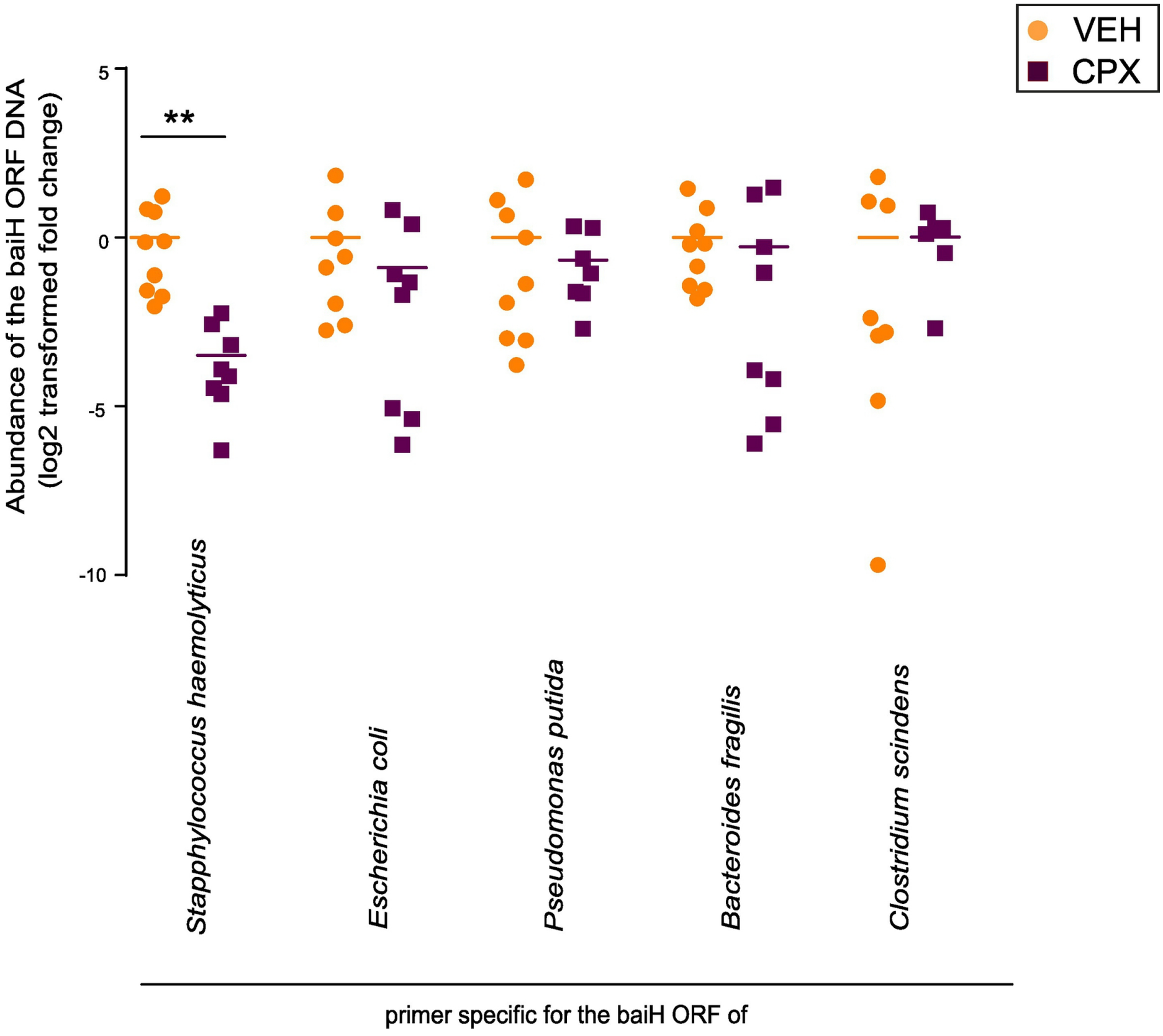
VEH
CPX
Abundance of the baiH ORF DNA
(log2 transformed fold change)
5
0
-5
-10
**
Stapphylococcus haemolyticus
Escherichia coli
Pseudomonas putida
Bacteroides fragilis
Clostridium scindens
primer specific for the baiH ORF of

Figure 7

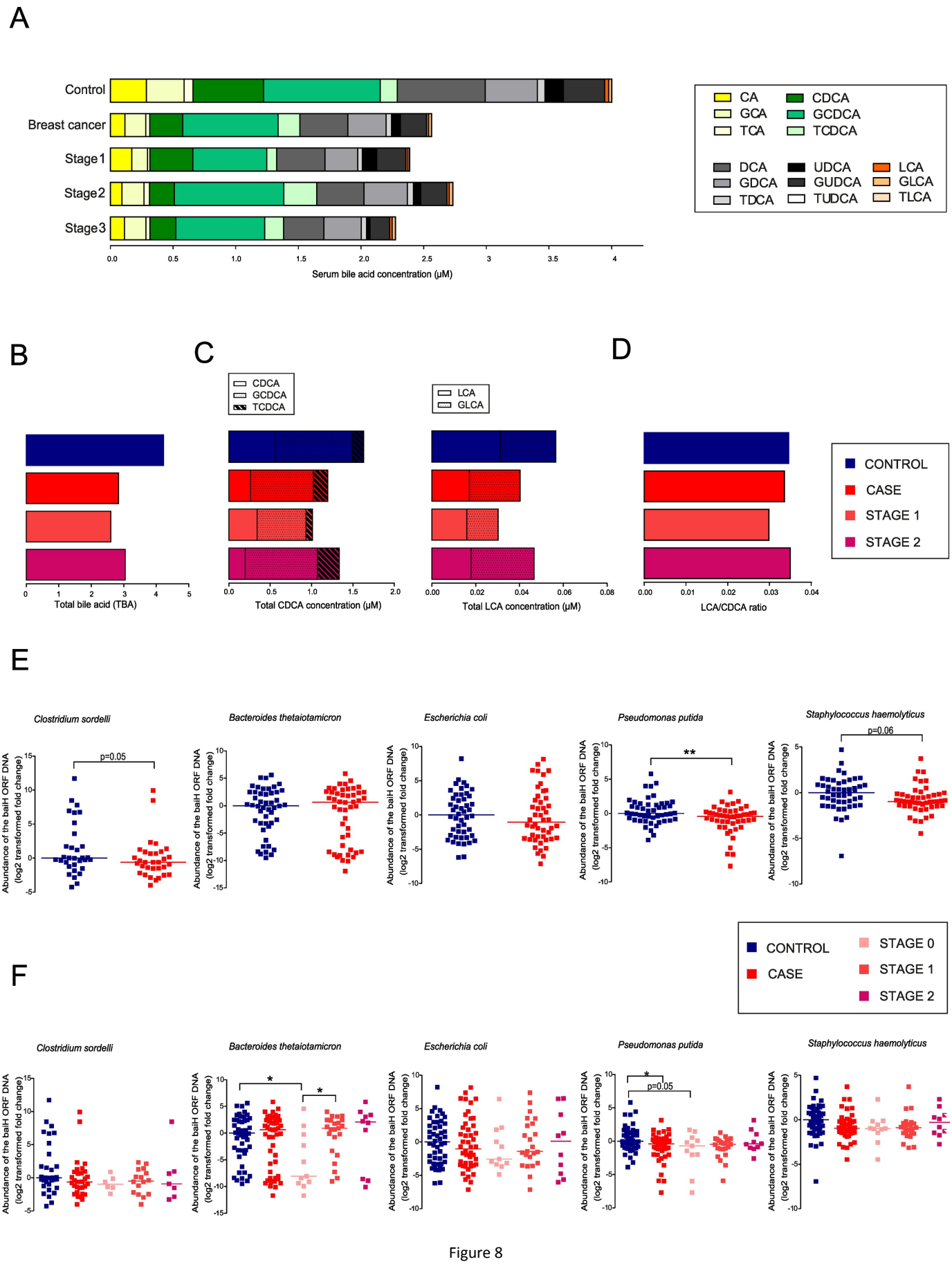
A
Control
Breast cancer
Stage 1
Stage 2
Stage 3
0.0 0.5 1.0 1.5 2.0 2.5 3 3.5 4
Serum bile acid concentration (μM)
CA
GCA
TCA
CDCA
GCDCA
TCDCA
DCA
GDCA
TDCA
UDCA
GUDCA
TUDCA
LCA
GLCA
TLCA
B
Total bile acid (TBA)
C
CDCA
GCDCA
TCDCA
Total CDCA concentration (μM)
LCA
GLCA
Total LCA concentration (μM)
D
LCA/CDCA ratio
CONTROL
CASE
STAGE 1
STAGE 2
E
Clostridium sordelli
Bacteroides thetaiotamicron
Escherichia coli
Pseudomonas putida
Staphylococcus haemolyticus
Abundance of the baiH ORF DNA (log2 transformed fold change)
p=0.05
**
p=0.06
CONTROL
CASE
STAGE 0
STAGE 1
STAGE 2
F
Clostridium sordelli
Bacteroides thetaiotamicron
Escherichia coli
Pseudomonas putida
Staphylococcus haemolyticus
Abundance of the baiH ORF DNA (log2 transformed fold change)
*
*
*
p=0.05

Figure 8